AIP | Journal of Applied Physics

Dynamics of polymer film formation during spin coating

Y. Mouhamad, P. Mokarian-Tabari, N. Clarke, R. A. L. Jones, and M. Geoghegan

Citation: Journal of Applied Physics **116**, 123513 (2014); doi: 10.1063/1.4896674
View online: http://dx.doi.org/10.1063/1.4896674
View Table of Contents: http://scitation.aip.org/content/aip/journal/jap/116/12?ver=pdfcov
Published by the AIP Publishing

Dynamics of polymer film formation during spin coating

Y. Mouhamad,[1] P. Mokarian-Tabari,[2] N. Clarke,[1] R. A. L. Jones,[1] and M. Geoghegan[1,a)]
[1]*Department of Physics and Astronomy, The University of Sheffield, Hicks Building, Hounsfield Road, Sheffield S3 7RH, United Kingdom*
[2]*Materials Research Group, Department of Chemistry and the Tyndall National Institute, University College Cork, Cork, Ireland*

(Received 24 May 2014; accepted 17 September 2014; published online 26 September 2014)

Standard models explaining the spin coating of polymer solutions generally fail to describe the early stages of film formation, when hydrodynamic forces control the solution behavior. Using *in situ* light scattering alongside theoretical and semi-empirical models, it is shown that inertial forces (which initially cause a vertical gradient in the radial solvent velocity within the film) play a significant role in the rate of thinning of the solution. The development of thickness as a function of time of a solute-free liquid (toluene) and a blend of polystyrene and poly(methyl methacrylate) cast from toluene were fitted to different models as a function of toluene partial pressure. In the case of the formation of the polymer blend film, a concentration-dependent (Huggins) viscosity formula was used to account for changes in viscosity during spin coating. A semi-empirical model is introduced, which permits calculation of the solvent evaporation rate and the temporal evolution of the solute volume fraction and solution viscosity.
[http://dx.doi.org/10.1063/1.4896674]

I. INTRODUCTION

Spin coating is a technique widely used to make polymer films. An excess amount of polymer solution is placed on a substrate, which is then rotated at typically 1000 to 5000 revolutions per minute (rpm) in order to spread the fluid by centrifugal force. Subsequently, the evaporation of the solvent thins the film. The technique is used in the manufacturing of CDs, and in microelectronic devices. A small change in the coating spin speed or on the concentration of the solution can lead to large changes in the final thickness. With the arrival of organic devices, considerable work has gone into controlling the morphology of polymer films. To do so, one can adjust the concentration of the solution, the polymer ratio, the spin speed, and, in addition, use thermal or solvent annealing techniques. In this way, it is possible to control the dynamics of film formation, which is intrinsically linked to the final structure of the film.

A full understanding of the mechanism of film formation would enable the temporal quantification of the polymer and the solvent concentrations. These provide valuable information to understand phase separation. The morphologies of spin-coated films depend on the dynamics, i.e., the quench depth can be controlled with the spin speed. The forces that govern the phase separation are negligible comparable to centrifugal forces; for this reason, phase separation does not influence the dynamics. However, interactions between polymer chains can alter the dynamics by changing the rheology of the solution.

The first mathematical analysis of spin coating was provided by Emslie, Bonner, and Peck (EBP),[1] who proposed a one-dimensional model describing the thinning of a non-volatile Newtonian fluid on an infinite rotating plate. The model is one dimensional because they assume that the flow is symmetric and neglects the radial dependence on the solvent content and the film thickness. These two assumptions considerably simplify the mathematical calculations; all the models discussed here respect these assumptions. The hydrodynamics of a rotating fluid with a velocity vector $\vec{v} = (v_r, v_\theta, v_z)$, an angular velocity ω, a viscosity η, and a density ρ are best described in cylindrical coordinates (r, θ, z). (Some of these terms are shown in Fig. 1.) A balance between the viscous forces and the centrifugal forces enables calculation of the radial velocity. Using the continuity equation, it was possible to obtain a differential equation in which thinning is only due to the centrifugal force. The work of EBP shows that centrifugal forces lead to a uniform film independently of the initial fluid distribution. The EBP model was further developed by Meyerhofer,[2] who considered a constant evaporation rate, based on the assumption of a uniform solvent distribution in the out-of-plane axis, z.

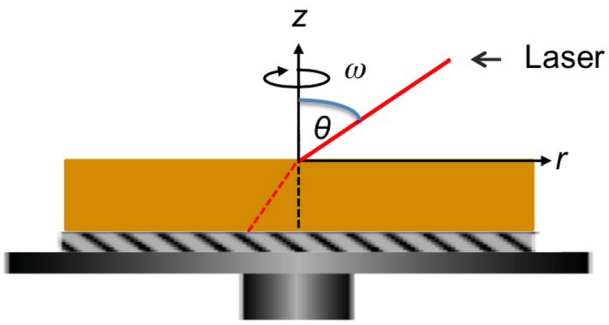

FIG. 1. Schematic diagram of a rotating polymer film, indicating the radial direction, r, the out-of-place direction, z, the incident laser angle, θ, and the angular rotation speed, ω.

a)Electronic mail: mark.geoghegan@sheffield.ac.uk

Meyerhofer's work showed that spin coating is a two-stage process. The initial stage lasts a few milliseconds. In this stage, the film thins mainly due to the radial convection outflow; in the second stage, the process is dominated by the solvent mass transfer, which is controlled by the solvent diffusion in the film and the solvent partial pressure. More detailed mathematical investigations have also been performed in which the concentration profile of solvent in the z direction using the convection-diffusion equation was included.[3] Here, the evaporation was assimilated into the solvent mass transfer, which is equal to the mass transfer coefficient multiplied by the difference between the solvent volume fraction at the surface of the film and the solvent volume fraction above the film. The thinning rate of the film is expressed using the kinematic boundary condition,

$$\frac{\partial h}{\partial t} = v_h - e_r, \tag{1}$$

where h is the thickness of the film, e_r is a constant evaporation rate, and $v_h = v_z(z = h)$ is the vertical velocity at the surface of the film. Equation (1) is a common result when working on the dynamics of spin coating and was calculated by several groups.[2–5] The thinning rate of a spin-coated film depends only on the vertical velocity of the fluid and the evaporation rate. The model predicts thinner films and longer drying times when the air above the film is saturated with solvent. Other experiments were performed which showed that when the overlaying layer is filled with a gas, interfacial shear increases the thinning rate.[6]

Because spin coating is a rapid process, much of the work performed to date on its dynamics is purely theoretical. This is due to the paucity of suitable *in situ* techniques to measure the film thickness. An important goal of experimental research was the prediction of the final thickness as a function of the angular velocity and the concentration of the solution. To this end, interferometry techniques have been used to monitor the thinning of a spin-coated sol-gel at various spin speeds in air and in saturated solvent vapor,[7] although these results were not compared to any mathematical model. Simple linear regression has been used to examine the thinning of poly(methyl methacrylate) (PMMA) films and determine the rate of evaporation.[8] The Meyerhofer model[2] was shown to be successful for the prediction of the late stage of the thinning of toluene, allowing a calculation of the evaporation rate during spin coating.[9] The evaporation rate was also calculated using the Meyerhofer model for the thinning rate of other organic solvents using an interferometric technique.[10]

The work presented here is a study of the dynamics of the spin coating of polymer films as a function of the solvent partial pressure and combines experimental data obtained using specular reflectivity with numerical modeling. The experimental set-up is identical to that used previously.[9,11,12] First, the dynamics of a solute-free liquid (toluene) is investigated, followed by a blend of polystyrene (PS) and PMMA, initially dissolved in toluene. Here, a semi-empirical model describing the dynamics of spin-coated films is presented and is compared to the one proposed by Reisfeld, Bankoff, and David (RBD).[5]

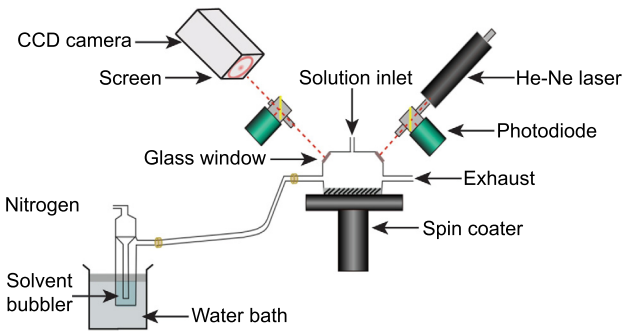

FIG. 2. Schematic diagram showing the experimental set-up used to control the pressure in the chamber and the instrumentation used to obtain the specular reflectivity data.

II. EXPERIMENTAL PROCEDURE

A He-Ne laser with a wavelength of 633 nm was mounted at 45° to a spin coater (Fig. 2). The intensities of the incoming and reflected beam were measured with two photodiodes and the specular reflectivity was calculated. A custom-made cell was used to control the solvent partial pressure above the film. The cell was fitted with two glass windows, which allowed the incident beam into the cell and the reflected beam out of it. The cell has three outlets: the first is for the deposition of the polymer solution, the second is for the ingress of solvent (toluene) vapor, and the third to exhaust it. 3 l min^{-1} of nitrogen was allowed to flow in a bubbler filled with toluene. The bubbler was immersed in a water bath, and a precise control of the solvent vapor in the cell was possible by controlling the temperature of the bath. The solvent vapor in the cell was related to the bath temperature by the Clausius-Clapeyron equation,

$$\frac{P(T)}{P(T_0)} = \exp\left(-\frac{\Delta H_v}{R}\left(\frac{1}{T_0} - \frac{1}{T}\right)\right), \tag{2}$$

where ΔH_v is the enthalpy of evaporation of the solvent, R is the gas constant, T_0 is the boiling point of the solvent (in K), and $P(T_0)$ and $P(T)$ are the solvent partial pressures at its boiling point and another (lower) absolute temperature, T, respectively. The films were cast on silicon wafers with a surface area of $\sim$1 cm^2. The silicon was cleaned using the RCA1 procedure, in which a mixture of water, hydrogen peroxide, and ammonium hydroxide in the proportion of 5:1:1 volume ratio was heated at 70 °C. The silicon pieces were immersed in the mixture for 10 min, then rinsed with deionized water, and dried under a nitrogen flow. Unless otherwise specified, all films were spun at 1000 rpm. The procedure used differed between spin coating a solute-free liquid and a polymer solution. In the first case, a substrate covered with toluene was enclosed in the cell for 1 min prior to spin coating. This procedure could not be used when coating a polymer solution as the solution dries at the edges of the substrate and creates ridges which affect the radial outflow and the quality of the data. In order to prevent this, the substrate was enclosed in the chamber and toluene vapor was allowed to flow in for 1 min, and only then was the polymer

solution deposited and then spun. The PS and PMMA were uniform with mass averaged molar masses of 96 and 106 kg mol^{-1} respectively, and both were purchased from Polymer Laboratories. The solution had a polymer concentration of 10% by weight, split equally between PS and PMMA. The thickness of the films after spin coating was measured using ellipsometry.

III. RESULTS AND DISCUSSION

Fig. 3(a) shows the specular reflectivity acquired when spin coating toluene at ambient atmosphere. At the early stage of the process, the convective forces lead to a rapid thickness change. At this stage, the time for a full reflectance cycle (including both constructive and destructive interference) is too small in comparison to the sampling period. Later on, the time required for a full reflection cycle is sufficient for the device to resolve the whole process, and the average intensity increases. Constructive interference (peaks) is obtained when the Bragg condition is satisfied, whereas troughs correspond to destructive interference. Between two successive peaks the thickness change is given by $\lambda/2n\sin\theta$, where $\lambda = 633$ nm, n is the refractive index of the solution, and θ ($=45°$) is the internal angle. Knowing the final thickness of the film, one can calculate the thickness of the film at every peak and so obtain a thickness profile. In the case of toluene, $n = 1.5$, and the change in thickness between two successive peaks is equal to 239 nm. When studying the case of polymer solutions we assume that the refractive index changes linearly as the solvent evaporates. Prior to and after coating, the refractive index is equal to the volume-weighted sum of the refractive indices of the solvent and polymers. The volume fraction of solvent in the final film is assumed to be zero. The refractive indices of PMMA and PS are 1.49 and 1.59, respectively. Fig. 3(b) shows the thickness as a function of time for a toluene layer at different partial pressures. The early stage of the process is not affected by the saturation of the chamber with vapor and the final time required for toluene to evaporate increases with increasing partial pressure.

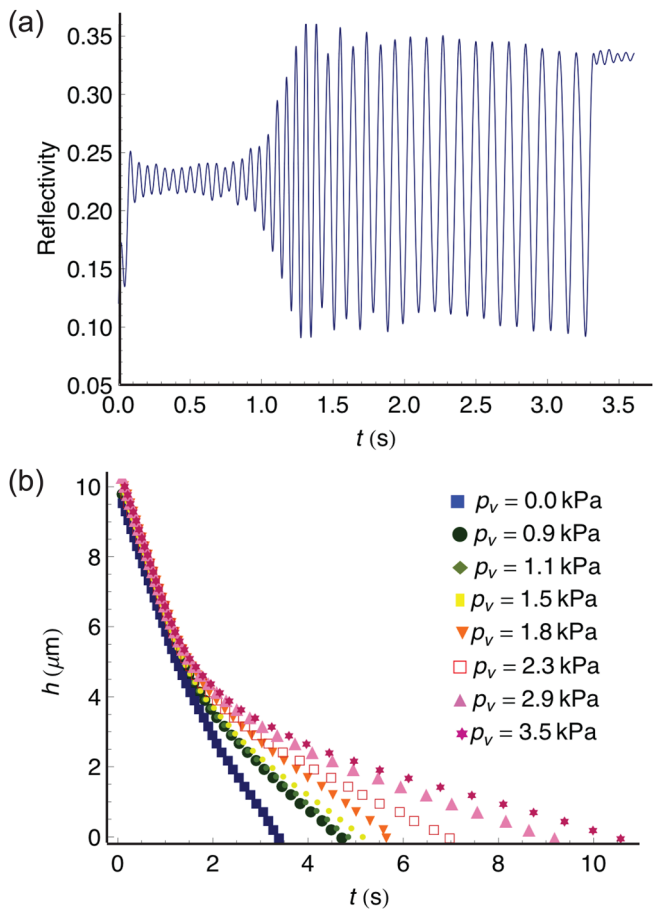

FIG. 3. (a) Specular reflectivity measured when studying the thinning of a toluene layer under ambient conditions (no toluene vapor environment). (b) Experimental thickness-time profile for toluene at various partial pressures.

A. Thinning of a solute-free liquid

Upon initial acceleration, the fluid spins at different speeds at the upper (air) interface and lower (substrate) interfaces. The degree to which this occurs is controlled by inertial forces. RBD[5] applied a lubrication and a perturbation theory to model the early stage of the spin coating, which is dominated by the radial outflow. Lubrication theory is applicable when studying the flow of a fluid in a geometry in which one dimension is significantly smaller than the others. The flow along the z axis is significantly smaller than the flow in the radial axis. A perturbation theory was applied and the velocity vector was expressed including a correction term to account for the inertial forces. The following differential equation was then obtained:

$$\frac{\partial h}{\partial t} = -\frac{2}{3}\left(\frac{\omega^2 h^3}{\eta_k} + \frac{\omega^4}{\eta_k^3}\left[\frac{5e_r\eta_k}{8}h^4 - \frac{34}{105}h^7\right]\right) - e_r, \quad (3)$$

where η_k is the kinematic viscosity. To describe the thinning of a spin-coated layer, Meyerhofer assumed that only two forces are exerted on the liquid: the centrifugal force and the viscous force. By assuming that these two forces balance each other, the following expression to describe the thinning of a spin coated layer was obtained:

$$\frac{\partial h}{\partial t} = -\frac{2\omega^2 h^3}{3\eta_k} - e_r. \quad (4)$$

As an alternative approach to analysing the present data, the model of Meyerhofer is extended in a semi-empirical form to include a correction term to the velocity in order to give a better description of the early stage of spin coating,

$$\frac{\partial h}{\partial t} = -\frac{2\omega^2 h^3}{3\eta_k} - \frac{B}{\exp(U^{t/\tau})} - e_r, \quad (5)$$

where B and U are fitting parameters which are functions of ω and η_k, but independent of h. In all of the data fitted, $\tau = 1$ s. B represents initial resistance to the thinning of the film due to the presence of the inertial force and $-B/\exp(U^{t/\tau})$ represents the rate at which resistance decreases. The fourth order Runge-Kutta method was used to fit the semi-empirical and RBD models. Fig. 4 shows that the fits obtained with the semi-empirical model are in agreement

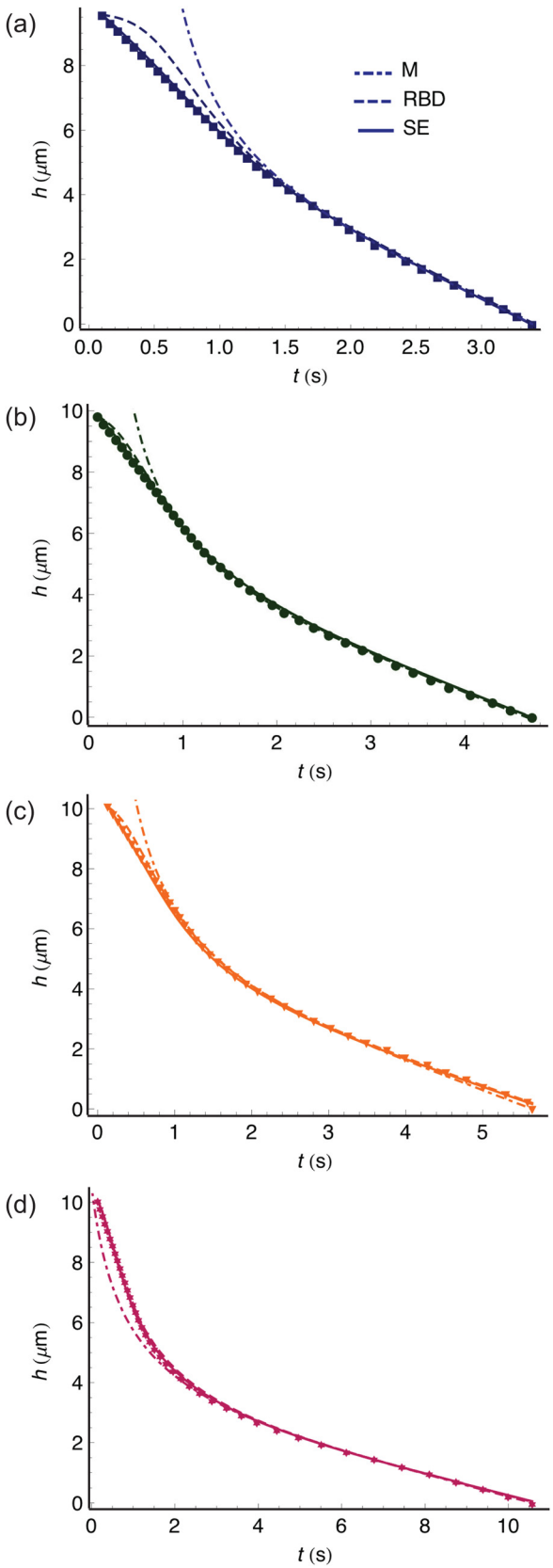

FIG. 4. Thickness-time profiles of toluene at different partial pressures, p_v. (a) $p_v = 0$ kPa, (b) $p_v = 0.9$ kPa, (c) $p_v = 1.8$ kPa, and (d) $p_v = 3.5$ kPa. The dotted lines are the experimental data; the solid lines are the fits to the semi-empirical model (SE); the dotted-dashed lines are the fits obtained with the Meyerhofer model (M); and the dashed lines are the fits to the RBD model.

with the experimental data for all partial pressures. The fits achieved with the Meyerhofer model are in agreement with the experimental data only at the late stage of the coating or at higher partial pressure where the hydrodynamic forces are negligible. Similar observations are made for the fits obtained with the RBD model at low partial pressure. However, as the partial pressure increases the quality of the fits obtained with the RBD model improves significantly.

In order to understand the quality of the fits, the axial velocity (v_z) terms for the three models are defined as

$$V_{\mathrm{RBD}} = -\frac{2}{3}\left(\frac{\omega^2 h^3}{\eta_{\mathrm{k}}} + \frac{\omega^4}{\eta_{\mathrm{k}}^3}\left[\frac{5e_{\mathrm{r}}\eta_{\mathrm{k}}}{8}h^4 - \frac{34}{105}h^7\right]\right), \quad (6)$$

$$V_{\mathrm{SE}} = -\frac{2\omega^2 h^3}{3\eta_{\mathrm{k}}} - \frac{B}{\exp(U^{t/\tau})}, \quad (7)$$

and

$$V_{\mathrm{M}} = -\frac{2\omega^2 h^3}{3\eta_{\mathrm{k}}}, \quad (8)$$

and are plotted in Fig. 5. In these equations, the subscripts RBD, M, and SE refer to the RBD, Meyerhofer, and semi-empirical models, respectively. The first terms in V_{RBD} and V_{SE} are equal to V_{M}, so that $V_{\mathrm{SE}} - V_{\mathrm{M}}$ is the semi-empirical model correction term and $V_{\mathrm{RBD}} - V_{\mathrm{M}}$ is the RBD correction term. Fig. 5(a) shows the axial velocities V_{RBD} and V_{SE}, which continuously decrease until a minimum is reached, and then they increase to zero in around two thirds of the time needed for the film to dry. This is in agreement with previous work,[6] where the modeling of the vertical velocity showed a rapid acceleration followed by a gradual deceleration. (The velocities in Fig. 5(a) are negative because the vertical velocity is in the negative direction of the ordinates. This means that the minimum in Fig. 5(a) is the maximum in the vertical velocity.) Fig. 5(b) shows that $|V_{\mathrm{M}}|$ decreases continuously to zero. At $t = 0$, $|V_{\mathrm{M}}|$ is significantly greater than $|V_{\mathrm{RBD}}|$ and $|V_{\mathrm{SE}}|$, which means that the Meyerhofer model predicts a larger radial outflow than the RBD and the semi-empirical models, as can be deduced from a comparison of Figs. 5(a) and 5(b). Fig. 5(c) shows the correction terms in the RBD and the semi-empirical models. The correction terms are positive because they represent the inertial forces which oppose to the thinning of the layer, whereas the vertical velocities are negative because the fluid moves in the direction of the negative z axis (Fig. 1). Note that the sum of the curves in Figs. 5(b) and 5(c) gives the curves in Fig. 5(a). The discrepancy between the Meyerhofer model and the experimental data is due to the Meyerhofer model not accounting for the initial acceleration of the fluid and therefore overestimating the radial outflow, as has been reported elsewhere.[6] In accordance with the improvement of the fits observed for thickness profiles with the RBD model in the presence of vapor, V_{SE} and V_{RBD} are indistinguishable at the highest partial pressure measured (Fig. 5(a)). It is interesting to note that the maximum in $|v_z|$ increases with partial pressure, and is due to the increase in the interfacial shear which enhances the rate of thinning as the partial pressure of toluene above the film increases.[6]

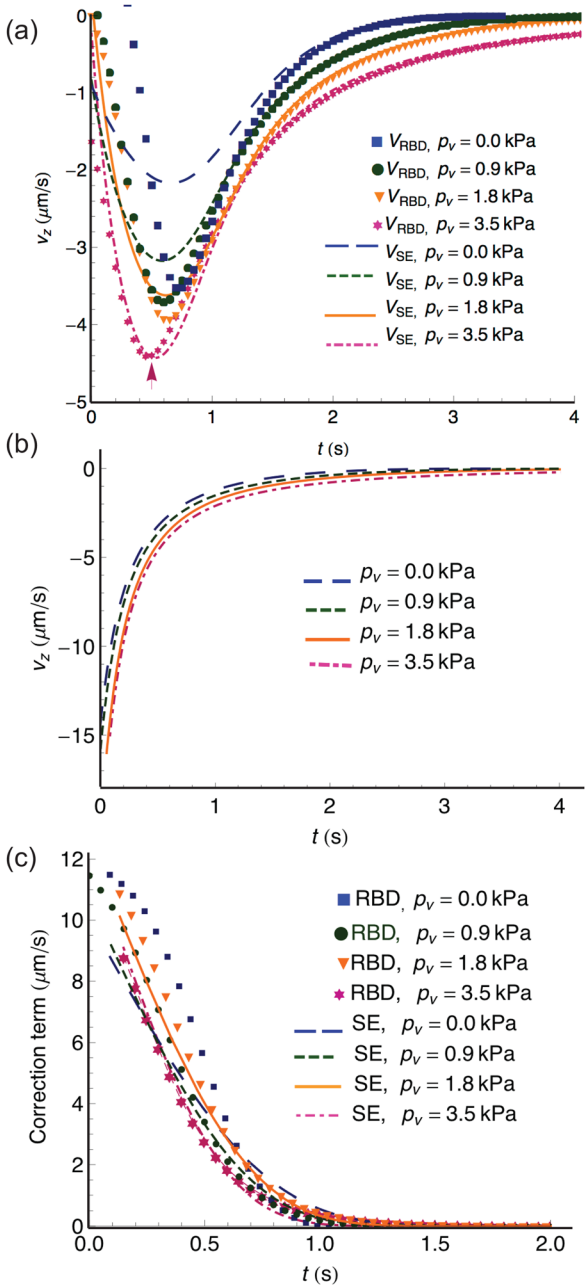

FIG. 5. (a) V_{SE} (lines) and V_{RBD} (points) at different partial pressures. (b) V_M at different partial pressures. (c) The correction terms (i.e., the curves in (b) subtracted from those in (a)), which illustrate the inertial forces at different partial pressures. The solid lines and the dashed lines show the semi-empirical and the RBD correction terms, respectively. The arrow in (a) indicates the maximum (absolute) vertical velocity for toluene spun at $v_p = 3.5$ kPa.

The term $V_{SE} - V_M = -B/\exp(U^{t/\tau})$ is empirical, and is likely to depend on thickness, rather than viscosity in these early stages. The intermediate stage, where hydrodynamic effects dominate, represents a balance between centrifugal effects (radial outflow or spreading) and viscosity (which resists the spreading), but before this stage, spreading dominates. Initially, the thinning rate increases with increasing partial pressure, as opposed to the late stage, which is evaporation dominated and the thinning rate decreases with increasing partial pressure. An analytical form of $h(t)$ is unavailable, but a formal derivation is unlikely to involve the integral of $-B/\exp(U^{t/\tau})$, which includes the exponential integral. In Fig. 4, the agreement of the data with the RBD model improves with increasing partial pressure. The shear due to the toluene vapor on the surface of the film results in an increase in the thinning rate.[6]

TABLE I. Values of t_c, t_{vmax}, and Re as a function of the partial pressure of toluene. t_{vmax} is the time at which the maximum in the velocity is reached, beyond which the magnitude of the inertial forces is negligible. The values of Re were calculated using the RBD model.

Partial pressure (kPa)	Re	t_{vmax}(s)	t_c(s)
3.5	1.56	0.51	0.58
2.6	1.60	0.51	0.55
2.3	1.65	0.62	0.61
1.8	1.79	0.61	0.58
1.5	1.77	0.51	0.58
1.2	1.85	0.57	0.60
0.8	1.87	0.58	0.61
No cell	2.20	0.65	0.64

The Reynolds numbers, Re, were calculated using the parameters obtained with the RBD model (Table I), and were between 1.56 and 2.20, which compares with Re = 13 for earlier work on naphthalene,[13] at a spin speed of $\omega = 1000$ rpm and $T = 343$ K, where a kinematic viscosity of $\eta_k = 9.6 \times 10^{-7}$ m^2/s (at $T = 353$ K) was used[14] to calculate the Reynolds number given the spinning speed, radius, and initial thickness. Small Re does not mean that viscous forces are dominant, but rather that the viscous and the centrifugal forces balance each other,[4] which occurs when

$$t_c = \frac{\eta_k}{h_0^2 \omega^2}. \tag{9}$$

At $t = t_c$, the vertical gradient in the radial solvent velocity reaches a steady state. For $t > t_c$, the velocity term is dominated by V_M and the inertial forces are negligible. (Experimentally this corresponds to the point at which $|v_z|$ reaches a maximum, as shown, for example, by the arrow in Fig. 5(a) for the toluene layer coated in an environment with $v_p = 3.5$ kPa.) Table I reports t_c and t_{vmax}, the time at which the velocity reaches its maximum; these two times are in good agreement, i.e., $t_c \approx t_{vmax}$. Once the vertical velocity (V_{RBD} or V_M) has reached a maximum the inertial forces are negligible. Rheological studies showed that t_c increases with Re,[6] as is also the case in the present work. t_c and t_{vmax} decrease as the partial pressure increases, which implies that the inertial forces becomes negligible earlier in the process as the partial pressure increases. This suggests that the quality of the fit obtained with the RBD model depends on the rate of decay of the inertial forces.

t_c decreases with increasing spin speed. To verify that the fits obtained with the RBD model improve with reduced inertial forces, we study the thinning of a toluene at 2000 and 3000 rpm (greater spin speeds reduce inertial forces). Fig. 6(a) shows the thickness as a function of time of a toluene layer spun at 2000 rpm and 3000 rpm and the corresponding fits for the RBD and the semi-empirical models. The fits obtained with the two models are in good agreement

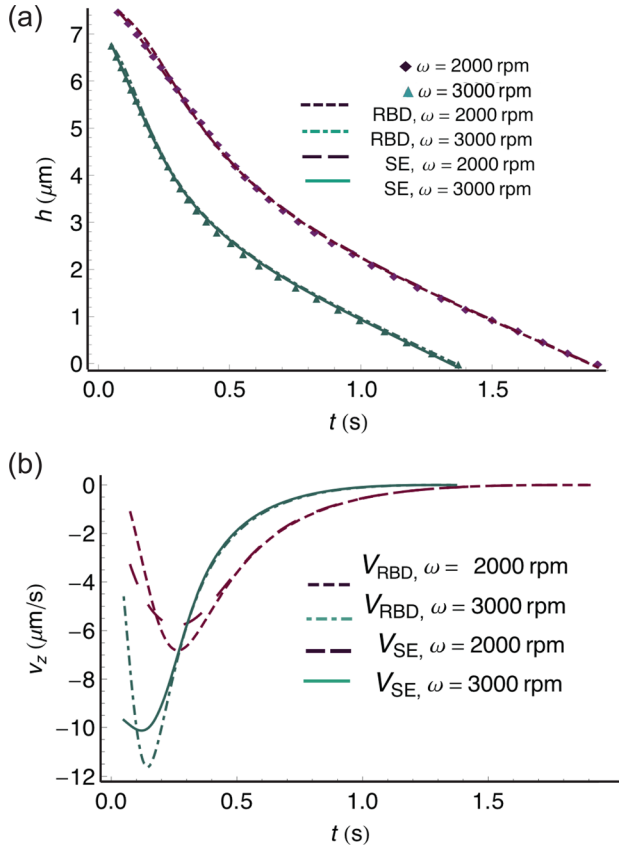

FIG. 6. (a) Thickness-time profiles for toluene cast at 2000 and 3000 rpm. The dashed lines are the fits obtained with the RBD model and the solid lines are the fits obtained with the semi-empirical model. (b) Axial velocity as a function of time; the solid lines show V_{SE} and the dashed lines V_{RBD}.

with the experimental data. Table II reports t_{vmax} and t_c; again they are in excellent agreement. We conclude that fits obtained with the RBD model improve when the inertial forces are weak and when they decay rapidly.

B. Thinning of polymer solutions

Polymer solutions can exhibit non-Newtonian behavior, i.e., the viscosity is dependent on the shear rate. In spin coating, the shear rate of the fluid increases with radial position and the fluid can exhibit non-Newtonian behavior during the process. Numerous groups have addressed this using different viscosity laws.[15–18] The behavior of film thinning of non-Newtonian fluids has now been modelled numerically.[19] However, the effect of evaporation and the consequences of height-dependent viscosity on thinning rate were not considered. Here, all the films are coated from semi-dilute polymer solutions. It was assumed that the flow is Newtonian, and so the models discussed in Sec. III A are all applicable. (The assumption of Newtonian flow is of course not generally true, but experiments on solutions of PS and PMMA have indicated that the shear rate is nearly proportional to shear stress, albeit at a small shear rate.[20]) As well as considering the rheology of the coated solution, it is necessary to account for the change in viscosity. The solvent evaporation leads to an abrupt increase in the viscosity, which causes the cessation of the radial flow and significantly reduces losses due to hydrodynamic forces. Meyerhofer was the first to include a time-dependent viscosity for a Newtonian fluid. The Huggins formula for viscosity is used to account for viscosity changes as the film thins so that

$$\eta_k = \eta_s(1 + [\eta]\phi + k'[\eta]\phi^2), \tag{10}$$

where $\phi = h_f/h(t)$ is the polymer volume fraction, $[\eta]$ is the intrinsic viscosity, k' is the Huggins constant, and η_s is the viscosity of the solvent.[21] For all solutions studied, the third term in Eq. (10) can be neglected. Equation (10) was substituted into Eqs. (3) and (5). The data are only fitted with the semi-empirical model and the RBD model because the Meyerhofer model does not provide fits of sufficient quality. Fig. 7(a) shows the fits for a PS:PMMA blend cast at 1000 rpm. The fits obtained with the semi-empirical model are in good agreement with the experimental data. Contrary to the case of toluene, the fits achieved with the RBD model do not improve with increasing partial pressure and spin speed (Fig. 7(d)). Similar results (not shown here) were obtained when investigating the dynamics of formation of single homopolymer films of both PS and PMMA cast from toluene at 2000 and 3000 rpm. Figs. 7(b) and 7(c) show the correction to the vertical velocity for the RBD and the semi-empirical model; a comparison of these two figures reveals that the RBD model underestimates the magnitude of the inertial forces and therefore overestimates the thinning rate, as a result the RBD correction term is four orders of magnitude smaller than the semi-empirical correction term. The large correction term in Fig. 7(c) may indicate that there is some other physics missing from the analysis, and may well indicate strong viscoelastic effects in the thinning, which would be incompatible with the assumption of Newtonian behavior.

It can be observed from Fig. 7(a) that at each partial pressure the last datum is not fitted and that the final thickness modelled is less than the experimental final thickness. Experimentally, the assumption of zero solvent remaining in the final film is shown to be inadequate at the end of the process. The polymer volume fraction and the viscosity are plotted only in the range where the experimental data are in agreement with the modeling, which is why the final volume fraction of polymer is less than unity. Figs. 8(a) and 8(b) show the polymer volume fraction and the relative viscosity, η_k/η_s. At all partial pressures studied, the polymer volume fraction curves are superimposed on each other in the hydrodynamics-dominated phase of the process; this is due to the fact that very little solvent is lost in this phase. In the second phase of the process where the evaporation is dominant, the polymer volume fraction increases at a slower rate when the partial pressure in the cell increases; this is because the evaporation rate decreases significantly (Fig. 8(d)).

TABLE II. t_c, t_{vmax}, and Re as a function of the spin speed. t_c was calculated using Eq. (9). t_{vmax} was determined graphically. The values of Re were calculated using the RBD model.

ω (rpm)	Re	t_{vmax} (s)	t_c (s)
1000	2.20	0.65	0.64
2000	1.8	0.26	0.25
3000	1.72	0.12	0.14

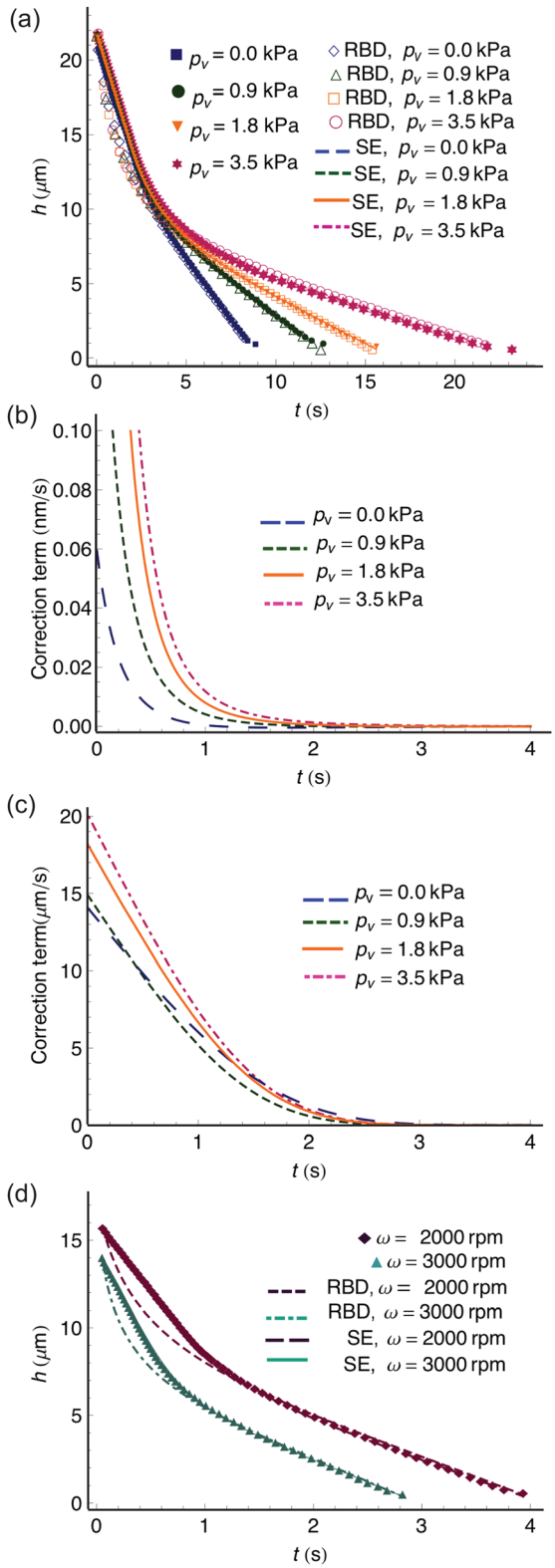

FIG. 7. (a) Thickness-time profiles for PS:PMMA films coated in different partial pressures. The RBD (b) and the semi-empirical (c) correction terms at different partial pressures. (d) Thickness-time profiles for PS:PMMA films cast at 2000 and 3000 rpm.

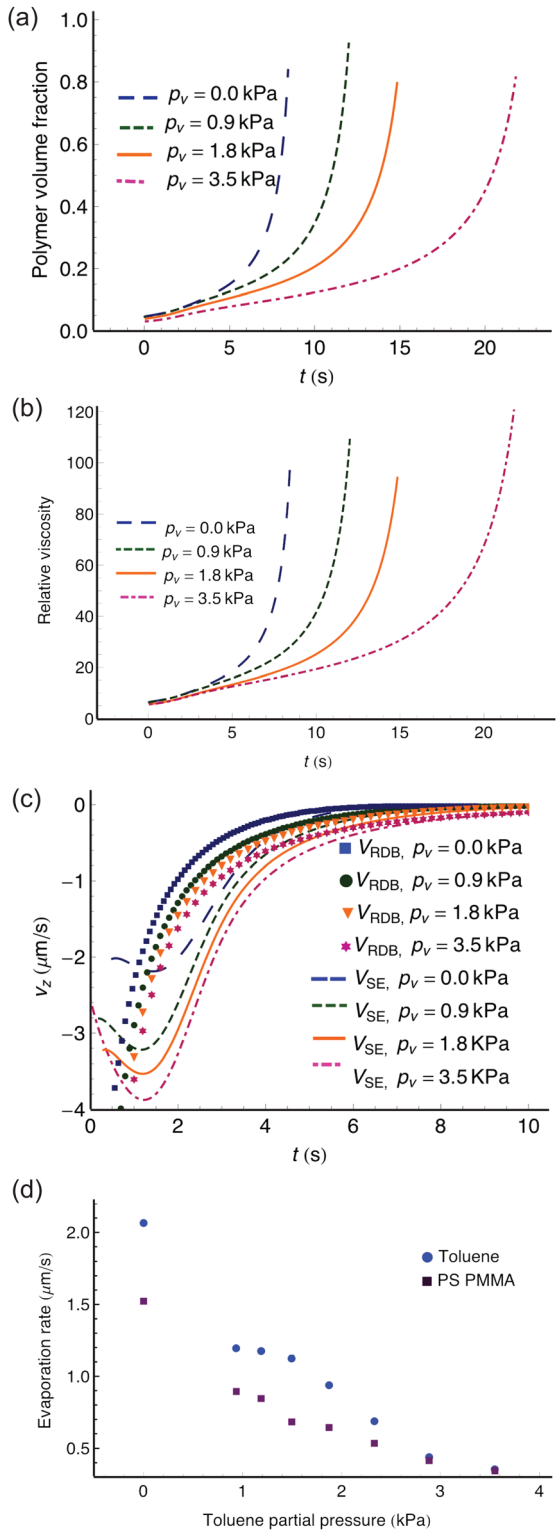

FIG. 8. (a) $\phi_{polymer}$, the polymer volume fraction in the film as a function of time at different partial pressures. (b) Relative viscosity, η_k/η_s, as a function of time at different partial pressures. (c) V_{SE} (lines) and V_{RBD} (points) at different partial pressures. (d) Evaporation rate as a function of partial pressure for toluene and PS:PMMA films.

Similar observations are made on the relative viscosity curves. According to Eq. (10), the viscosity is linearly dependent on the concentration, which is valid only for relatively dilute polymer solutions. One would expect the viscosity to depend on the concentration with a higher power once the polymer concentration is greater than the entanglement concentration. The agreement between the data and Eq. (10) lies in the fact that spin coating is a two-stage process. Comparing Figs. 8(b) and 8(c), one can see that the rate of

increase of the relative viscosity is significantly greater once the vertical velocity is small. Therefore, the fact that Eq. (10) underestimates the viscosity does not matter because the radial outflow is negligible. From the numerical modeling, we find that the initial polymer solution has a (dynamic) viscosity of 3.6 mPa s, which is significantly less than the ranges obtained in other experiments (whereby solvents other than toluene were investigated), where solutions with viscosities of 1.4–7.4 Pa s were measured in one case,[17] and 0.012–0.11 Pa s in another.[22] The low viscosities determined in the present calculations support the assumption of a Newtonian fluid.

Solvent evaporation is driven by two phenomena: the diffusion of the solvent molecules in the film and the solvent partial pressure above the film. In the case of toluene, the evaporation rates shown in Fig. 8(d) were calculated by taking the means of the rates obtained using the semi-empirical, the Meyerhofer, and RBD models. The three different models converge at long times, and so are in good agreement; it therefore makes sense to plot the average of the different evaporation rates. In a similar way, the evaporation rates for the PS:PMMA blend films are the average of the rates calculated with the RBD and the semi-empirical models, and these are also shown in Fig. 8(d). The evaporation rates of toluene in a solute-free layer and in PS:PMMA films decrease with increasing partial pressure and are equal at the highest partial pressure, as has been reported elsewhere.[3] At a given partial pressure, the rate of evaporation of toluene in PS:PMMA films is less than the evaporation of toluene in a toluene liquid film. This is because in the former case the solvent molecules have to diffuse in the films and thus experience a resistance to their migration to the film-air interface where evaporation takes place. At high partial pressures, the evaporation rate of toluene in a solute-free layer is equal to the evaporation of toluene in a PS:PMMA film. This implies that at low partial pressure the evaporation rate is dominated by the solvent diffusion in the film, while at high partial pressure the phenomenon is dominated by the solvent vapor above the film.

IV. CONCLUSIONS

The thinning of a solute-free toluene layer and the thinning of a polymer solution of a blend of polystyrene and poly(methyl methacrylate) dissolved in toluene were studied. It was shown that the Meyerhofer model fails to account for the inertial forces experienced by the fluid in the early stage of the coating. The RBD model gives a good description of the dynamics of a rapidly thinning solute-free layer. The inertial forces were accounted for by a semi-empirical model, which is in agreement with the experimental data for both the thinning of a solute-free liquid and the thinning of a polymer solution.

ACKNOWLEDGMENTS

We thank the Engineering and Physical Sciences Research Council for providing support under Grant No. EP/E04591X/01. Technical support from Mr. Simon Dixon and Mr. Paul Kemp-Russell is also gratefully acknowledged.

[1]A. G. Emslie, F. T. Bonner, and L. G. Peck, J. Appl. Phys. **29**, 858 (1958).
[2]D. Meyerhofer, J. Appl. Phys. **49**, 3993 (1978).
[3]D. E. Bornside, C. W. Macosko, and L. E. Scriven, J. Appl. Phys. **66**, 5185 (1989).
[4]B. G. Higgins, Phys. Fluids **29**, 3522 (1986).
[5]B. Reisfeld, S. G. Bankoff, and S. H. Davis, J. Appl. Phys. **70**, 5258 (1991).
[6]T. J. Rehg and B. G. Higgins, Phys. Fluids **31**, 1360 (1988).
[7]F. Horowitz, E. Yeatman, E. Dawnay, and A. Fardad, J. Phys. III France **3**, 2059 (1993).
[8]D. E. Haas, J. N. Quijada, S. J. Picone, and D. P. Birnie, in *Sol-Gel Optics V*, edited by B. Dunn, E. Pope, H. K. Schmidt, and M. Yamane (SPIE, Bellingham, WA, 2000), pp. 280–284.
[9]P. Mokarian-Tabari, M. Geoghegan, J. R. Howse, S. Y. Heriot, R. L. Thompson, and R. A. L. Jones, Eur. Phys. J. E **33**, 283 (2010).
[10]D. P. Birnie and M. Manley, Phys. Fluids **9**, 870 (1997).
[11]P. C. Jukes, S. Y. Heriot, J. S. Sharp, and R. A. L. Jones, Macromolecules **38**, 2030 (2005).
[12]S. Y. Heriot and R. A. L. Jones, Nature Mater. **4**, 782 (2005).
[13]F. Kreith, J. H. Taylor, and J. P. Chong, J. Heat Transfer **81**, 95 (1959).
[14]S. D. Ravikovich, Zh. Fiz. Khim. **24**, 524 (1950).
[15]A. Acrivos, M. J. Shah, and E. E. Petersen, AIChE J. **6**, 312 (1960).
[16]P. J. Carreau, Trans. Soc. Rheol. **16**, 99 (1972).
[17]S. A. Jenekhe, Polym. Eng. Sci. **23**, 830 (1983).
[18]S. A. Jenekhe and S. B. Schuldt, Ind. Eng. Chem. Fundam. **23**, 432 (1984).
[19]J. P. F. Charpin, M. Lombe, and T. G. Myers, Phys. Rev. E **76**, 016312 (2007).
[20]S. R. Vashishtha, N. Chand, and S. A. R. Hashmi, Indian J. Chem. Technol. **9**, 316 (2002).
[21]M. L. Huggins, J. Am. Chem. Soc. **64**, 2716 (1942).
[22]J. H. Lai, Polym. Eng. Sci. **19**, 1117 (1979).